Reanalysis of offshore T-joint fatigue life predictions based on a complete weld profile model.

E. Lozano-Minguez [a,*], F. P. Brennan [a], A. J. Kolios [a]

[a] Department of Offshore, Process & Energy Engineering, Whittle Building (B52), Cranfield University, United Kingdom, MK43 0AL.

[*]Corresponding author. Tel.: +44 1234750111

E-mail address: e.lozanominguez@cranfield.ac.uk (E. Lozano-Minguez)

ABSTRACT

A comparison between the fatigue life predictions obtained by the stress concentration factors (SCFs) of 3D solid finite element (FE) models considering the weldment and the existing SCF parametric equations for tubular T-joints, is presented in this paper. From the study carried out, it was concluded that the existing parametric equations for predicting hot spot SCFs are very conservative and insufficient to be used for optimisation. SCFs should be carried out by modelling 3D solid joints which include the weldment and should be based on notch stresses measured on the external surface at the weld toe. The Offshore and Marine Renewable Energy industry could significantly reduce their investment costs using contemporary FE models, since slight overestimations of the SCF results in a corresponding large reduction in predicted service life.

KEYWORDS

Stress Concentration Factors, Hot Spot Stress, Notch Stress, Fatigue life predictions, Tubular T-joints, Offshore support structures.

1. Introduction

Marine and offshore structures are subjected to environmental and operational loads with corresponding cyclic stresses which will in time degrade mechanical properties; hence, fatigue damage assessment is crucial for estimating service life. Steel tubular welded elements are widely used in marine and offshore structures because of their relative high strength, non-directional bending strength and lower drag coefficient. The changes of section and the welds at the intersection result in modifications of the stress distribution, causing high stress concentrations and making the structures susceptible to fatigue induced failure.

The first recommendations for the design of tubular joints against fatigue based on the use of the Stress-life (S-N) curve approach, which relates the stress range ($\Delta\sigma$) at a point under consideration to the number of cycles (N) to failure, were given by the American Petroleum Institute (API) and the American Welding Society (AWS) in 1972 **[1]**. The first S-N curves based on the hot spot stress (HSS) of the joint were called the X curve in the two American documents, API RP 2A **[2]** and AWS D1.1-72 **[3]**. The HSS definition was drafted by the review panel of the United Kingdom Offshore Steels Research Project (UKOSRP) and adopted by the UK Department of Energy (DEn) Guidance Notes **[4]** and states that it is the value calculated by the extrapolation to the weld toe of the maximum principal stresses at a distance a and b. The data used in obtaining the S-N curve were composed mainly of fillet-welded plate data and some small-scale tests on tubular joints tested

in air under constant amplitude **[1, 5]**. The 2nd edition of the UK DEn Guidance Notes **[6]** recommended the Q curve, which is based on the data generated by Marshall **[7, 8]**, Smedley **[9]** and Gurney **[10]**. Since this curve was first published two major revisions have taken place. The first revision was in 1984, when results from the UKOSRP and the European Coal and Steel Community (ECSC) sponsored research programme highlighted that the Q curve could be unconservative under certain conditions **[5]**. The S-N curve recommended in this revision became known as the T curve. Ref. **[1]** explains that a total of 64 T-, X- and K-joint test results were used to obtain the T curve. More specifically, the T-curve was formulated from the mean curve to the data from a 32 mm chord wall thickness curve less two standard deviations of data from 16 mm chord wall thickness, representing a confidence level of 97.7%. It is recommended for joints in air or seawater where adequate protection against corrosion has been provided. The formulation of the T-curve was also based on the HSS. The second revision was in 1996, when a significant amount of new data became available on the fatigue behaviour of welded tubular joints **[11]**. The new curve for tubular joints was designated the T' curve. Ref. **[11]** explains that a total of 59 T-, Y-, X- and K-joints of 16 mm were used to obtain the T' curve, because this was the largest subset of data with the widest range of joint geometries and loading modes. This second revision retained the hot spot stress definition used previously. A preliminary assessment of the data showed that the slope (m) of the mean $\log_{10}N$ vs. $\log_{10}S$ line had a value which was very close to 3, and a fixed value of m equal to 3 was retained for consistency with the earlier Guidance.

For tubular welded joints, much research has been carried out into the estimation of the magnitude of the hot spot stress range. Some empirical equations were based on the strain gauge measurements of numerous tests on tubular joints under the three principal modes of loading – axial, in-plane bending (IPB) and out-plane bending (OPB); examples are the Wordsworth & Smedley equations **[12]** for predicting SCFs of T-, Y- and X-joints published in 1978, the Wordsworth formulae **[13]** for K- and KT-joints published in 1981, and the Lloyd's Register (LR) equations **[14]** proposed in 1991 for T-, Y-, X-, K- and KT-joints. All those tests however, did not consider the geometry of the weld profile. The hot spot stresses were derived following DEn recommendations, using maximum principal stresses from outside the notch zone. The high costs of testing scaled steel models led most of the studies to use shell finite element (FE) models for deriving the SCF parametric equations for all three load cases, for example: the equations proposed by Kuang et al. **[15]** for T-, K- and TK-joints in 1975; the Gibstein equations **[16]** derived in 1978 for tubular T-joints; the Efthymiou & Durkin parametric formulae **[17]** for T-, Y- and K-joints with emphasis on overlapped joints published in 1985; the Hellier et al. equations **[18]** proposed in 1990 for Y- and T-joints; and the set of parametric equations derived by Chang & Dover **[19, 20]** in 1998 for predicting stress distributions along the intersections of tubular T-, Y-, X- and DT-joints. Most of these studies measured the stresses at the mid-section of the brace-chord intersection without considering the effect of a weld fillet; excepting the Efthymiou & Durkin's models, where welds were modelled using three-dimensional sixteen node shell elements in the brace and the chord, and eight node shell elements in the weld regions. All SCFs presented in that publication were obtained by extrapolating maximum principal stresses to the weld toes in accordance with DEn recommendations.

The existing hot spot SCF parametric equations are mostly several decades old. Therefore, this paper aims to show that offshore and marine renewable application practices need to be based on contemporary FE models if the objective is to achieve optimum design avoiding unnecessary costs of over-conservatism. For this purpose, a comparison between the fatigue life predictions obtained

by the SCFs of 3D solid FE models considering the weldment, and the existing SCF parametric equations for tubular T-joints was made. The validation of the 3D solid FE models with the weldment was carried out by analysing the results obtained by 3D solid and 3D shell FE models without the weldment, as they were used in obtaining the existing parametric equations.

Fig. 1. Validation of the 3D solid FE models with the weldment.

2. Finite Element Analyses (FEAs).

Following this comprehensive literature review, the FEA package ABAQUS/CAE was used for modelling tubular T-joints in order to analytically obtain hot spot stresses for calculating stress concentration factors.

2.1. Shell FE tubular T-joint models

2.1.1. Modelling and meshing

Shell elements are commonly used for tubular joint stress analysis; for this reason initial models were formed by thin four-node quadrilateral elements. Models were subjected to axial, IPB and OPB load cases. The stresses were measured at the mid-section, without considering the effect of a weld fillet. The SCFs were estimated by dividing the maximum principal stress obtained at the brace/chord intersection by the appropriate nominal stress. Maximum principal stresses were selected for this research to maintain consistency with DEn recommendations and the existing SCF parametric studies. For axial loading, the nominal stress was defined as the total applied load divided by the hollow cross-sectional area of the brace. For IPB, the nominal stress was calculated from the Euler–Bernoulli Beam Theory using a moment arm measured from the brace end along its outer surface to the crown position. For OPB, nominal stress was also derived from the Euler–Bernoulli Beam Theory but the moment arm measured to the saddle position. For all models, all degrees of freedom were fixed at the chord ends.

Only one joint geometry will be presented but several geometries have been modelled, the magnitude of the results is different but the trend is the same. The chosen geometric ratios for the models are shown in Fig. 2, and were selected with the purpose of comparing the effectiveness of these models with the study shown in Ref. **[19]**. All these ratios are within the validity range of the different parametric equations pointed out in Section 1.

Fig. 2. Geometric notation and selected values for the tubular T-joints.

In order to reduce computational time, the mesh of all the models is characterised by fine elements near the intersection and coarser elements in regions where the stresses are more evenly distributed, as can be observed in Fig. 3. Elements elongated or distorted were avoided. T-joints with a brace length of about $0.4L$ were used in order to avoid the effect of short brace length **[20]**. Chord lengths greater than $6D$ were used to ensure that stresses at the brace/chord intersection were not affected by the boundary conditions **[21]**. The density, Young's modulus and Poisson's ratio were taken to be 7850 kg/m^3, 207 GPa and 0.3 respectively.

Fig. 3. Typical mesh used to model the T-joint.

2.1.2. Mesh validation

A convergence test was carried out aiming to verify that the meshes used for this research were sufficiently fine to accurately predict the SCFs. Four meshes with 32, 64, 112, and 160 elements respectively around the joint intersection were analysed. Comparison of SCF values (see Table 1) shows a good convergence. The finest mesh, which has 160 elements around the intersection with a side length of 9.22 mm, was selected for the rest of the analysis as there is acceptable compromise between computational time and accuracy. It has to be noted that the T-joint was subjected to different axial loads in order to prove that the SCF does not depend on the magnitude of the load.

Table 1 Comparison between the SCFs along the intersection from coarse to fine meshes.

Axial Loading [N/mm2]	Number of elements	CHORD		BRACE	
		Crown	Saddle	Crown	Saddle
1	**16x2**	1.805	4.960	2.054	6.175
4	**32x2**	1.792	5.460	2.424	7.338
4	**56x2**	1.788	5.661	2.622	8.012
10	**80x2**	1.788	5.805	2.681	8.218

2.1.3. Results comparison

Once the mesh was selected, the T-joint model was subjected to IPB loading and OPB loading. The higher stress concentration is located at the saddle for axial and OPB cases, and close to the crown for IPB case, as may be appreciated from Fig. 4.

Fig. 4. SCF distributions along the T-joint intersection for the different load cases.

The shell FE results were compared with the results presented in Ref. **[19]** and the solutions for the different parametric equations outlined in Section 1, which are presented in Table 2.

Table 2 SCFs comparison.

		CHORD		BRACE	
		CROWN	SADDLE	CROWN	SADDLE
Axial	**Kuang et al. Eq.[15]**		6.106		8.553
	Efthymiou et al. Eq.[17]	2.203	6.602	2.400	6.407
	Hellier et al. Eq.[18]	2.833	7.047	2.579	8.109
	Lloyds's Register of Shipping Eq.[22]	2.596	5.960	1.883	4.707
	Chang et al. [19]	2.199	7.497	2.813	9.171
	Shell FE results	**1.788**	**5.805**	**2.681**	**8.218**
IPB	**Kuang et al. Eq.[15]**	1.633		2.169	
	Efthymiou et al. Eq.[17]	2.175		2.494	
	Hellier et al. Eq.[18]	2.505	0.000	3.035	0.087
	Lloyds's Register of Shipping Eq.[22]	1.895		1.067	
	Chang et al. [19]	2.578	0.056	3.330	0.181
	Shell FE results	**2.020**	**0.064**	**2.865**	**0.247**
OPB	**Kuang et al. Eq.[15]**		4.457		5.586
	Efthymiou et al. Eq.[17]		5.060		5.391
	Hellier et al. Eq.[18]	0.000	5.348	0.000	4.522
	Lloyds's Register of Shipping Eq.[22]		4.380		3.390

Chang et al. [19]	0.177	5.553	0.434	6.621
Shell FE results	**0.092**	**4.591**	**0.391**	**6.097**

If these results are only compared with the results presented by Ref. **[19]**, it seems that SCFs are underestimated at the chord saddle and brace saddle for axial loading, and at the chord saddle for OPB loading. However, for the rest of the load cases, the results are of the same magnitude; small differences are attributed to the finest mesh.

Taking into consideration all the different SCF values, it is difficult to characterise if the obtained results were under- or over-predicted because of some rather high variations. For instance, LR's SCF at the brace saddle for axial loading is 4.707 while for Kuang et al. it is 8.552. It is our view that the FEA results are reasonable and hence acceptable since they are within this range.

2.2. Solid FE tubular T-joint models

Solid models were characterised by eight-node hexahedral elements. Models were subjected to axial, IPB and OPB load cases, and both chord ends were rigidly fixed. The SCFs for the solid FE models without fillet weld were estimated directly from the values obtained at the brace/chord intersection in the same manner as for the Shell FE models, except that the maximum principal stresses were measured at the external surface. The mechanical properties and the restrictions of the brace and chord lengths used for the shell FE models of Section 2.1.1 were also applied on the solid FE models without the weldment.

When producing the meshing of the 3D solid models, the number of elements around the joint intersection was 160 as the solid FE models were going to be validated with the shell FE models, and a convergence test was carried out aiming to verify the number of elements through thickness. Comparison of SCF values shows a good convergence (see Table 3). Ten elements through the thickness proved to have an acceptable compromise between computational time and accuracy.

Table 3 Comparison between the SCFs along the thickness from coarse to fine meshes

Number of elements through thickness	Intersection	
	Crown	Saddle
5	2.338	7.829
7	2.616	8.613
9	2.828	9.195
10	2.917	9.434
11	2.958	9.545

Table 4 shows the results obtained for the same tubular T-joint geometry modelled with solid elements instead of shells.

Table 4 Solid FE SCFs.

Load case	Number of elements	Intersection	
		Crown	Saddle
Axial	**80x2**	2.917	9.434
IPB	**80x2**	3.199	0.184
OPB	**80x2**	0.294	6.815

As observed for the shell FE models, the higher stress concentration is located at the saddle for axial and OPB cases, and close to the crown for the IPB case. If the shell FEA results are compared with these results, it can be observed that there is an increase of the SCF of 14.8% for axial loading and 11.8% for OPB loading at the saddle. At the crown, there is an increase in the SCF of 11.7% for IPB loading. It is reasonable that the solid SCFs are slightly higher, since the shell results are measured at the mid-section, whereas the solid results are measured on the external surface.

2.3. Complete weld profile Solid FE tubular T-joint models

2.3.1. Modelling and meshing

The mesh conditions, the mechanical properties, the geometric ratios, and the restrictions of the brace and chord lengths used for the shell and solid FE models explained in Section 2.1.1 were also applied to the complete weld profile Solid FE tubular T-joint models.

For modelling the weldment, the recommendations for complete joint penetration (CJP) groove welds provided by the AWS Structural Welding Code **[23]** were applied. It is necessary to define the coordinates of nodes A, B and D (shown in Table 5 and Fig. 5) in order to incorporate the weldment within the tubular joint.

Table 5 Prequalified joint dimensions and groove angles for CJP groove welds in tubular T-Connections with 90º<Ψ<120º.

	Saddle		Crown	
	min	**max**	**min**	**max**
$\boldsymbol{\omega}$	45°	90°	10°	90°
$\mathbb{R}$	2mm	$\phi \leq 45°$ 8mm $\phi > 45°$ 6mm	2mm	$\phi \leq 45°$ 8mm $\phi > 45°$ 8mm
$\boldsymbol{c}$	0mm	2mm	0mm	2mm
$\boldsymbol{\phi}$	37.5°		37.5°	60°
$\boldsymbol{F}$	0mm	t/2 mm	0mm	t/2 mm
$\boldsymbol{t_w}$	≥ t mm		≥ t mm	
$\boldsymbol{F + t_w}$	≥ t mm		≥ t mm	

Fig. 5. Prequalified joint details for CJP groove welds in tubular T-Connections.

The coordinates of node A may be defined by the brace, chord and intersection equations shown in Fig. 6 as:

$$Node\ A = \{r\cos\theta\ , \sqrt{(r\sin\theta)^2 - (r^2 - R^2)}, r\sin\theta\} \quad \textbf{(1)}$$

Fig. 6. Coordinate system.

In the same way, the coordinates of node A' are defined as:

$$Node\ A' = \{(r-t)\cos\theta\ , \sqrt{\left((r-t)\sin\theta\right)^2 - ((r-t)^2 - R^2)}, (r-t)\sin\theta\} \quad \textbf{(2)}$$

Assuming that the root opening ($\mathbb{R}$) has a constant value equal to 4 mm, which is an intermediate value in the range of validity, the coordinates of node B' can be derived from the coordinates of node A'. To simplify some calculations, it has been considered that a root face (c) equals 0 mm because the dihedral angle (Ψ) will be equivalent to the sum of the joint included angle (ϕ) and the end preparation angle (ω). Considering an end preparation angle of 50º, which is the intermediate value of the range of validity at the crown, the coordinates of node B are defined as:

$$Node\ B = \{r\cos\theta\ , \sqrt{\left((r-t)\sin\theta\right)^2 - ((r-t)^2 - R^2)} + \mathbb{R} + \frac{t}{\tan\omega}, r\sin\theta\} \quad \textbf{(3)}$$

Assuming a fillet weld size (F) equal to half the brace thickness (t), which is its maximum value, the coordinates of node D are defined as:

$$Node\ D = \{(r+F)\cos\theta\ , \sqrt{R^2 - \left((r+F)\cos\theta\right)^2}, (r+F)\sin\theta\} \quad \textbf{(4)}$$

The dihedral angle is defined as:

$$\Psi = \pi - \arctan\frac{y_D}{\sqrt{R^2 - {y_D}^2}} \quad \textbf{(5)}$$

To calculate the weldment curvature (R_w) is necessary to define some parameters, shown in Fig. 7 as:

Fig. 7. Parametric definitions for the calculation of R_w.

$$h = \sqrt{(y_A - y_D)^2 - (x_D - x_A)^2} \quad \textbf{(6)}$$

$$q = \sqrt{(y_B - y_D)^2 - (x_D - x_B)^2} \quad \textbf{(7)}$$

Using the sine rule:

$$\zeta = \arcsin(\frac{h}{q}\sin\Psi) \quad \textbf{(8)}$$

Finally, the weldment curvature is expressed as:

$$R_w = \frac{\frac{q}{2}}{\cos\delta} = \frac{\frac{q}{2}}{\cos(\frac{\pi}{2} - \zeta)} \quad \textbf{(9)}$$

The final configuration is shown in Fig. 8.

Fig. 8. Complete profile solid FE model.

2.3.2. Complete weld profile Solid FE results.

For the complete weld profile solid FE model, two different SCFs may be obtained, distinguished by the stress analysis results selected as reference, as Fig. 9 shows.

Fig. 9. Different stresses.

There is no general agreement on the value of the distances from the weld toe for obtaining the HSS; the extrapolation regions defined by Ref. **[24]**, and adopted by the UKOSRP and the ECSC

Technical Working Party on Tubular joint Testing are shown in Fig. 10. This definition of HSS was selected because there must be consistency between the generation of the design S-N curve and the SCF.

Fig. 10. Location of strain gauges for linear extrapolation to weld toe.

The notch stress is the peak stress, which is situated at the weld toe region. The notch stress concept is attractive since it is a real stress; in contrast to the extrapolated conceptual HSS, which incorporates the effects of joint geometry but neglects the influence of the weld.

Table 6 shows both hot spot and notch SCF values obtained by measuring the maximum principal stresses at the external surface.

Table 6 Hot Spot and Notch SCFs for the T-joint.

		Number of	CHORD		BRACE	
Stress	Load case	elements	Crown	Saddle	Crown	Saddle
	Axial	80x2	2.070	5.019	1.365	5.049
HS	IPB	80x2	1.642	0.082	1.685	0.107
	OPB	80x2	0.053	3.813	0.285	3.502
	Axial	80x2	2.510	6.962	1.504	5.256
Notch	IPB	80x2	2.295	0.149	1.679	0.102
	OPB	80x2	0.174	5.168	0.239	3.671

As expected, both hot spot and notch SCF values are lower than the intersection values of the previous shell and solid FE models, since the change in the section is less sharp, i.e. the weldment reduces stress levels because the change in the direction of force flow is more progressive.

Generally notch SCFs are higher than hot spot SCFs, although the increase is not proportional; for instance, the increase at the chord saddle for OPB loading is 35.5% while at the brace saddle for axial loading is 4.1%. Therefore, selecting the hot spot stress as a reference could lead to designing a structure very conservatively, since an important reduction of the stress concentration could be achieved through the improvements on the weld profile and this is not taken into account. For example, employing safety factors over the brace crown SCF for IPB loading would produce a very high overestimation since the notch SCF is smaller than the hot spot SCF.

3. Discussion

In order to know to what extent the slight variations on the SCF values affect the fatigue life predictions, an assessment using the HSS T' curve was carried out. The T' design S-N curve for tubular joints in air with a chord wall thickness of 16 mm is expressed below [11]:

$$log_{10}N = 12.476 - 3\ log_{10}\Delta\sigma \qquad \text{for } N < 10^7 \qquad \textbf{(10)}$$

$$log_{10}N = 16.127 - 5\ .\ log_{10}\Delta\sigma \qquad \text{for } N > 10^7 \qquad \textbf{(11)}$$

The decrease in fatigue strength for thicker joints, which is known as the "thickness effect", is a generally accepted trend; however, the scale of the decrease and the reasons for the shorter lives of thicker joints are still the subject of some controversy. The main reasons given for thicker sections

having lower fatigue resistance within the same stress range are: the "geometric effect", where the decrease is primarily caused by the increased local weld toe stresses caused by the change in weld geometry of the thicker joints; the “volumetric effect”, where simply having more material implies a greater likelihood of having more defects; and the “stress gradient effect”, which applies to thin sections under bending and the associated steep stress decay gradient which has been demonstrated to make thinner sections relatively strong against fatigue. The thickness correction recommended for the T' curve is of the form **[25]**:

$$\Delta\sigma = \Delta\sigma_o \cdot (\frac{16}{T})^{0.3} \quad \textbf{(12)}$$

The hot spot SCF values obtained by the solid FEA models with the weldment, which are the most representative models, were used as references for being compared with the Efthymiou & Durkin SCFs, which were the only parametric equations derived by shell FE models taking into account the weldment, and the SCFs obtained with the solid FE models without weldment. A nominal stress of 20 MPa was considered for the comparison in order to be within the range of cycles for a service life of 20 years **[26]**. Table 7 shows the results for the most critical points: at the chord saddle for axial and OPB loading, and at the chord crown for IPB loading.

Table 7 Comparison between fatigue life predictions at the chord for all load cases.

	CHORD		σ_{nom} (MPa)	SCF	$\Delta\sigma_o$ (MPa)	THICKNESS CORRECT. $\Delta\sigma$(MPa)	N (cycles)
AXIAL	SADDLE	Efthymiou & Durkin	20	6.602	132.04	104.51	2.62E+06
		Solid FE model without weldment	20	9.434	188.68	149.34	8.98E+05
		Solid FE model with weldment (HSS)	20	5.019	100.38	79.45	5.97E+06
IPB	CROWN	Efthymiou & Durkin	20	2.175	43.5	34.43	2.77E+08
		Solid FE model without weldment	20	3.199	63.98	50.64	4.02E+07
		Solid FE model with weldment (HSS)	20	1.642	32.84	25.99	1.13E+09
OPB	SADDLE	Efthymiou & Durkin	20	5.060	101.2	80.10	5.82E+06
		Solid FE model without weldment	20	6.815	136.3	107.88	2.38E+06
		Solid FE model with weldment (HSS)	20	3.813	76.26	60.36	1.67E+07

Considering 5 million cycles per year, which corresponds to an average period of 6.3 sec – i.e. 100 million cycles in 20 years’ service life **[26]**, these variations would represent an overestimation of between 0.64 and 217.74 years (see Fig. 11). These results clearly show that even slight overestimations of the SCFs will represent a great reduction on service lives, since the scale is logarithmic. This reduction on the service life affects the design, i.e. structures would be oversized.

Fig. 11. Service life comparison.

It should be noted that all authors of the studies reviewed in Section 1 agree that the SCF parametric equations must be different depending on the type of joint and applied load. The mode of loading affects the fatigue strength; however, the T' curve does not make any distinction between joint types or applied loads. This effect of the mode of loading on the fatigue strengths means that the S-N curve approach may not be suitable to predict the fatigue life for all joint geometries and modes of loading.

Aiming to observe how these under-predictions of the service life affect investment costs, the chord thickness was reduced until the SCFs of the complete profile solid FE model reached approximately the same values as Efthymiou & Durkin's SCFs for the previous thickness. The total reduction of the T-joint was 12.24%, and the SCFs are shown in Table 8.

Table 8 SCFs of the complete profile solid FE model with the thickness reduction.

	Efthymiou & Durkin's SCF T_{ref}	Complete profile solid FE model $0.86\,T_{ref}$
Axial loading	6.602	6.466
IPB loading	2.175	1.596
OPB loading	5.060	4.744

All the SCF parametric equations for all three load cases proposed by Kuang et al. [15], Gibstein [16], Efthymiou & Durkin [17], Hellier et al. [18], and Chang & Dover [19, 20] for tubular T-, Y-, X-, K-, TK- and DT-joints have the same type of constraints. Therefore, assuming that this reduction is representative for all the different joint intersections; although the magnitude of the total reduction will vary across different structural configurations.

In 2012, the average investment cost of offshore wind farms was €3.43m per MW **[27]**, the foundations represent around 22% of this cost **[28]** (€0.75m per MW). Assuming that the material costs of the legs and bracings of the jacket are about one third of the total foundation [29], which could be reduced by 12.24%, around €30,787 per MW could be saved. Approximately 1 GW of Offshore Wind was connected to the grid in Europe during 2012 **[27]**; hence, notionally (assuming a steel jacket construction which was not the case) we could deduce that approximately €30.8m could have been reduced from this investment cost without any real effect in structural performance but by simply modelling the weld profile effect on Hot-Spot Stress. Whereas these installations have been largely monopile structures to date, in future there is likely to be an increased number of steel jacket structures as larger turbines and deeper water conditions are encountered. It is therefore important to remember that small over-predictions of the SCFs could inadvertently result in very large increase in investment costs.

4. Conclusion

From the study carried out, it can be concluded that the existing parametric equations for predicting hot spot SCFs are very conservative and not useful for optimisation. SCFs should be carried out by modelling solid joints which include the weldment, and should be based on notch stresses measured on the external surface at the weld toe, since slight overestimations of the SCFs represent a great reduction in predicated service lives. Use of SCFs obtained from the complete weld profile FE models allow design of structures with the same service life but reduced wall thickness, reducing the capital cost of an offshore wind farm; or extend their effective service life. Furthermore, new S-N curves based on fatigue tests of contemporary materials using representative geometries and manufacturing techniques, which make a distinction between joint types and applied loads, are required in view of the fact that the mode of loading also affects fatigue strength.

References

[1] UEG, Underwater Engineering Group. Design of tubular joints for offshore structures, vol. 2. Norwich: UEG Offshore Resarch; 1985.

[2] API, American Petroleum Institute. API RP 2A-Recommended Practice for Planning, Designing and Constructing Fixed Offshore Platforms; 1972.

[3] AWS, American Welding Society. Structural Welding Code-Steel AWS D1.1-72; 1972.

[4] DEn, Department of Energy. Offshore Installations: Guidance on Design and Construction. London : HMSO; 1984.

[5] HMSO, Her Majesty's Stationery Office. Background to new fatigue design guidance for steel welded joints in offshore structures. London: Report of the Department of Energy Guidance Notes Revision Drafting Panel; 1984.

[6] DEn, Department of Energy. Offshore Installations: Guidance on design, construction and certification. London: HMSO Publications; 1977.

[7] Marshall PW. General Considerations for Tubular Joint Design. Welding in Offshore Constructions-International Conference, The Welding Institute; 1974. Paper 2.

[8] Marshall PW. Basic considerations for Tubular Joint Design in Offshore Construction. WRC Bulletin 193; 1974.

[9] Smedley GP. Welded Steel Structures-The Avoidance of Fatigue and Fracture. University of California: Structures in the Ocean Conference; 1973.

[10] Gurney TR, Maddox SJ. A Re-Analysis of Fatigue Data for Welded Joints in Steel. Welding Research International; 1973; vol.3, n.4.

[11] HSE, Health and Safety Executive. Background to new fatigue guidance for steel joints and connections in offshore structures. Offshore Technology Report - OTH 920390, prepared by Failure Control Ltd and MaTSU; 1999.

[12] Wordsworth AC, Smedley GP. Stress concentrations at unstiffened tubular joints. Cambridge, UK: European Offshore Steels Research Seminar; 1978. Paper 31

[13] Wordsworth AC. Stress concentration factors at K and KT tubular joints. London: Fatigue in Offshore Structural Steels Conference; 1981.

[14] Smedley PA, Fisher PJ. Stress concentration factors for simple tubular joints. Edinburgh: Proceedings of the First International Offshore and Polar Engineering Conference; 1991.

[15] Kuang JG, Potvin AB, Leick RD. Stress concentration in tubular joints. Texas: Offshore Technology Conference; 1975.

[16] Gibstein MB. Parametric stress analysis of T-joints. Cambridge, UK: European Offshore Steels Research Seminar; 1978. Paper 26.

[17] Efthymiou M, Durkin S. Stress concentrations in T/Y and gap/overlap K-joints. Amsterdam: Behaviour of Offshore Structures, Elsevier Science Publishers; 1985.

[18] Hellier AK, Connolly MP, Dover WD. Stress concentration factors for tubular Y- and T-joints. London: International Journal of Fatigue; 1990; vol. 12, No. 1, pp 13-23

[19] Chang E, Dover WD. Prediction of stress distributions along the intersection of tubular Y and T-joints. London: International Journal of Fatigue; 1998; vol. 21, pp. 361-381.

[20] Chang E, Dover WD. Parametric equations to predict stress distributions along the intersection of tubular X and DT-joints. London: International Journal of Fatigue; 1999; vol. 21, pp. 619-635.

[21] Yong-Bo S, Zhi-Fu D, Seng-Tjhen L. Prediction of hot spot stress distribution for tubular K-joints under basic loading. Singapore: Journal of constructional Steel Research; 2009; vol. 65, pp.2011-2026.

[22] LR, Lloyd's Register of Shipping. Stress concentration factors for simple tubular joints. Assessment of Existing and development of new parametric formulae. London: Health and Safety Executive - Offshore Technology Report; 1997.

[23] AWS, American Welding Society. Structural Welding Code - Steel. Miami: ANSI AWS D1.1/D1.1M:2006; 2006.

[24] Irvine NM. Review of Stress Analysis Techniques used in UKOSRP. London: Fatigue in Offshore Structural Steels. Proceedings of Conference at the Institute of Civil Engineers. Thomas Telford; 1981.

[25] HSE, Health & Safety Executive. Fatigue Design Curves for Welded Joints in Air & Seawater Under Variable Amplitude Loading. Offshore Technology report OTH 1999 058, prepared by Failure Control Engineering & Materials Consultants; 2000.

[26] DNV, Det Norske Veritas. Recommended Practice DNV-RP-C203 Fatigue Design of offshore steel structures; 2011.

[27] EWEA, European Wind Energy Association. The European offshore wind industry - key trends and statistics 2012. Available from: http://www.ewea.org/fileadmin/files/library/publications/statistics/European_offshore_statistics_2012.pdf; 2013.

[28] DECC, Department of Energy & Climate Change. Cost of and financial support for offshore wind. Available from: http://webarchive.nationalarchives.gov.uk/+/http:/www.berr.gov.uk/files/file51142.pdf; 2009.

[29] Seidel M. Jacket substructures for the REpower 5M wind turbine. Berlin: Conference Proceedings European Offshore Wind 2007; 2007.

Nomenclature

a, b	Extrapolation points
A, B, D	Weldment nodes
API	American Petroleum Institute
AWS	American Welding Society
c	Root face
CJP	Complete Joint Penetration
d	Brace diameter
D	Chord diameter
DEn	Department of Energy
ECSC	European Coal and Steel Community
F	Fillet weld size
FE	Finite Element
HSS	Hot Spot Stress
IPB	In-Plane Bending
l	Brace length
L	Chord length
LR	Lloyd's Register
m	Slope of the S-N curve
N	Number of cycles
OPB	Out-Plane Bending
r	Brace radius
R	Chord radius
$\mathbb{R}$	Root opening
R_w	Weldment curvature
SCF	Stress Concentration Factor
S-N	Stress-life
t	Brace thickness
T	Chord thickness
t_w	Theoretical weld
UKOSRP	United Kingdom Offshore Steels Research Project
$\Delta\sigma$	Stress Range
σ_{nom}	Nominal stress
φ	Brace to chord inclination angle
α	Chord stub slenderness ratio
β	Brace to chord diameter ratio
γ	Chord wall slenderness ratio
τ	Brace to chord thickness ratio
θ	Angle measured around intersection from saddle toe
Ψ	Dihedral angle
ω	End preparation angle
ϕ	Joint included angle

Figure 1

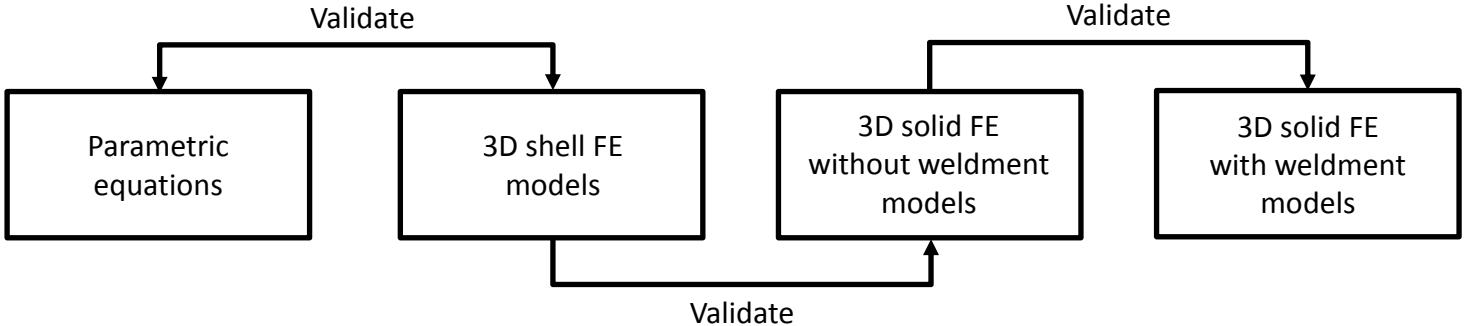
Validate
Parametric equations
3D shell FE models
Validate
3D solid FE without weldment models
Validate
3D solid FE with weldment models

Figure 2

Geometric ratios:

$$\alpha = \frac{2L}{D} = 10.39$$

$$\beta = \frac{d}{D} = 0.5$$

$$\gamma = \frac{D}{2T} = 12.9$$

$$\tau = \frac{t}{T} = 0.5$$

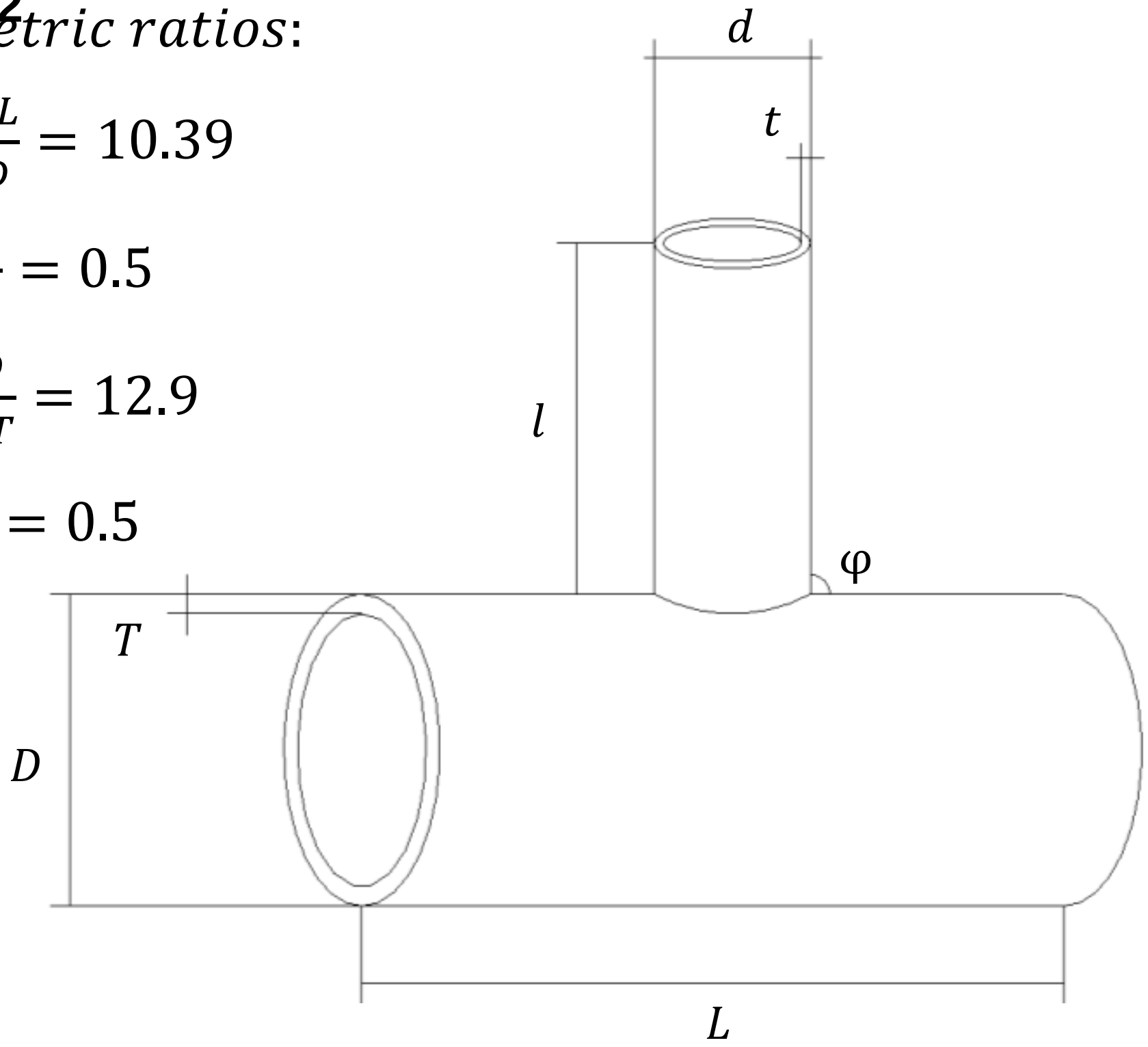

Figure 3

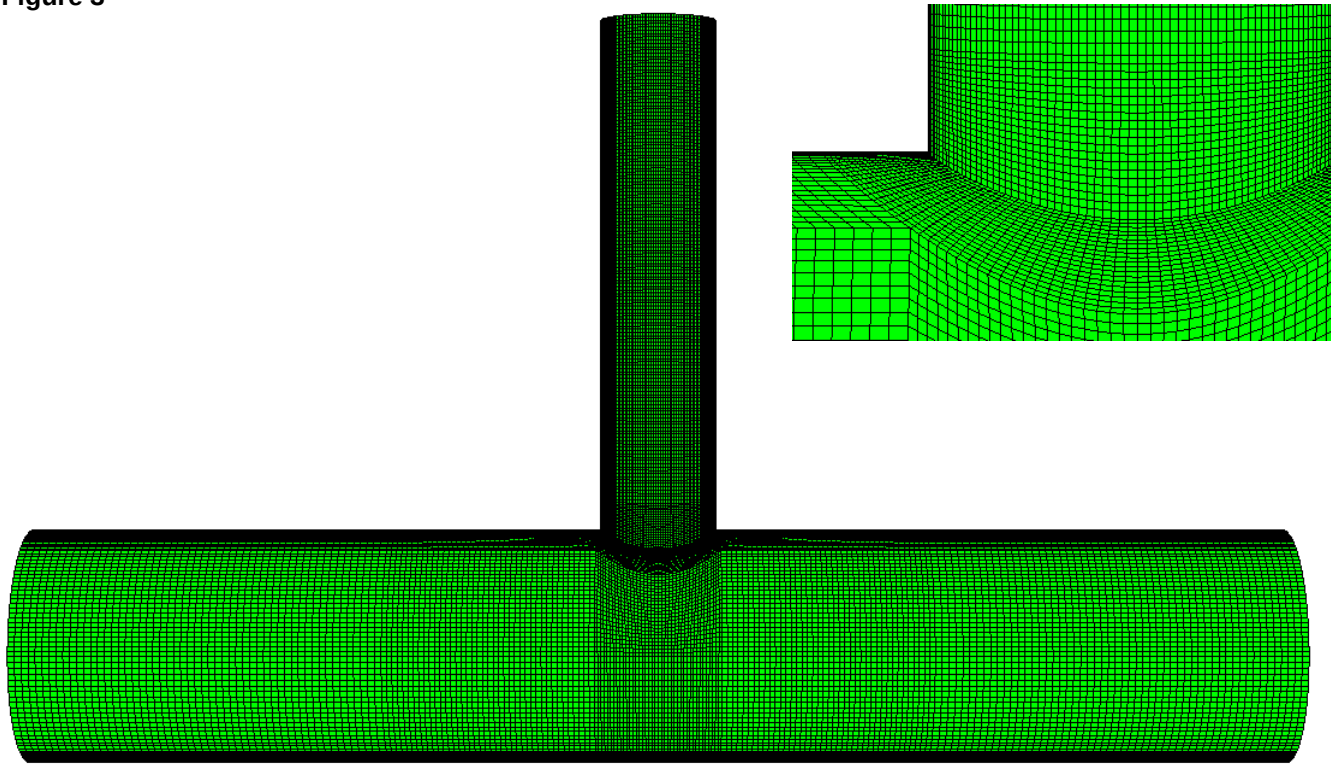

Figure 4

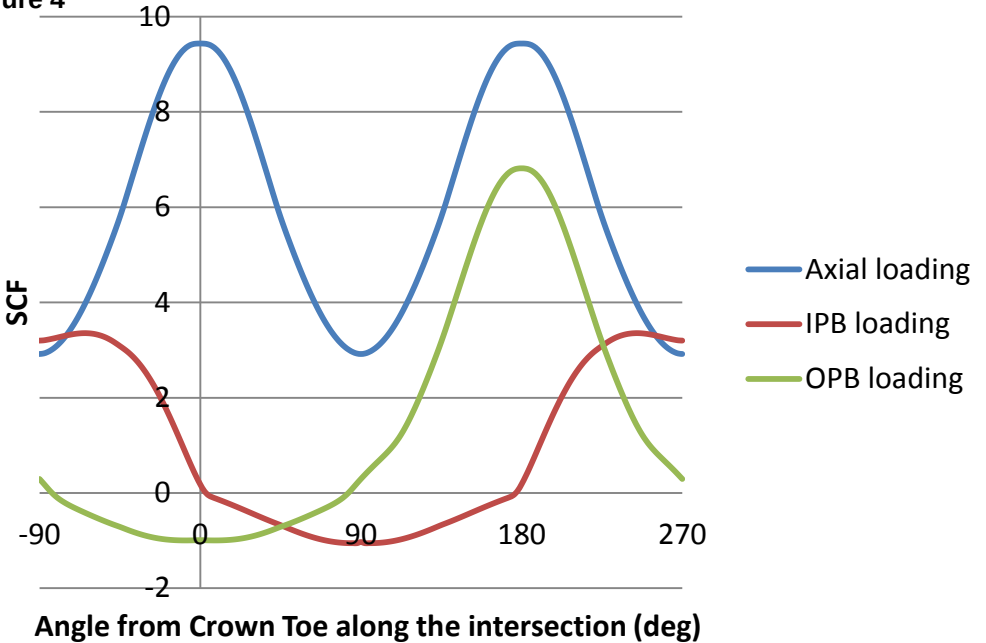
10
8
6
4
2
0
-2
SCF
-90
0
90
180
270
Angle from Crown Toe along the intersection (deg)
Axial loading
IPB loading
OPB loading

Figure 5

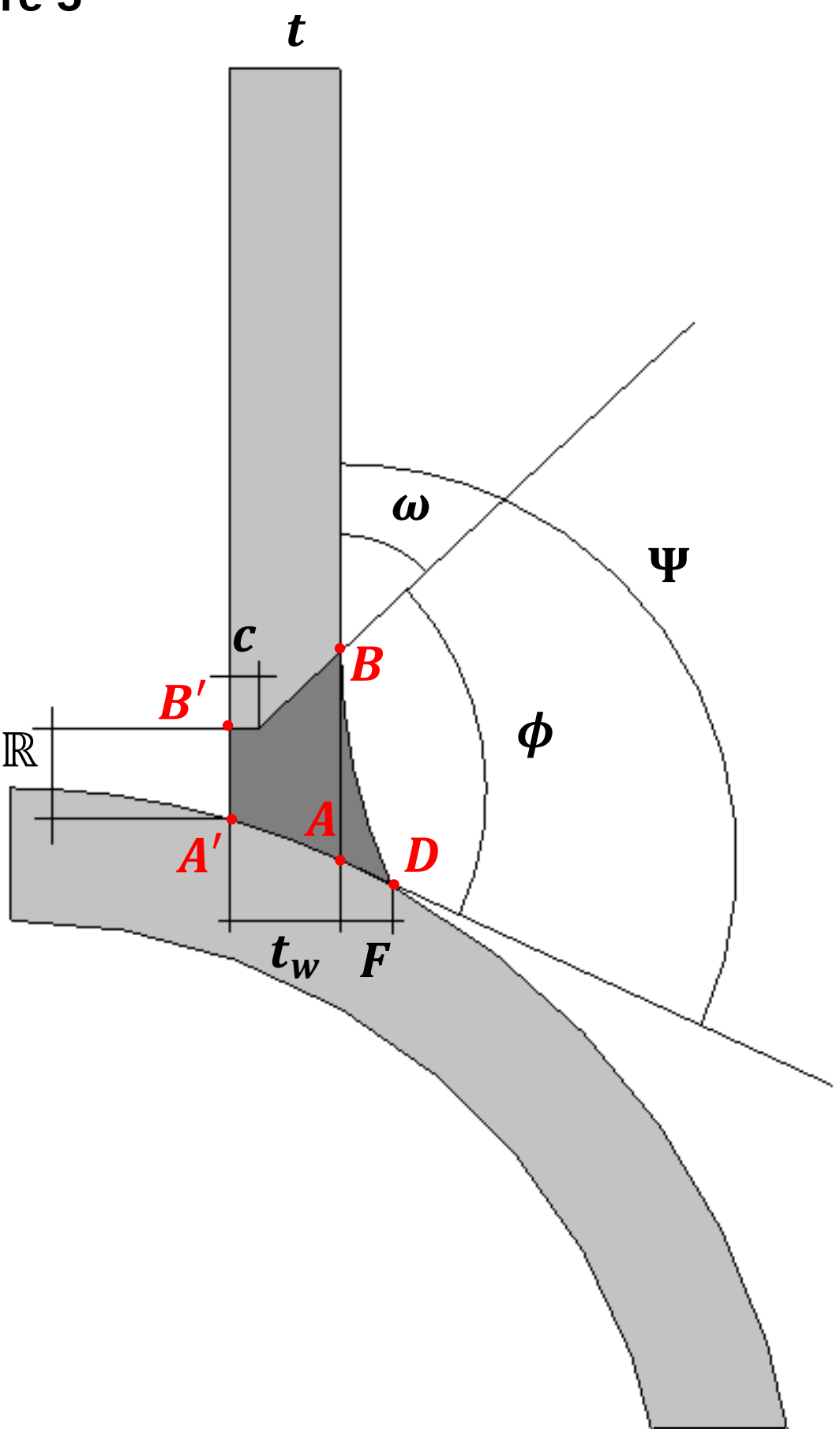

Figure 6

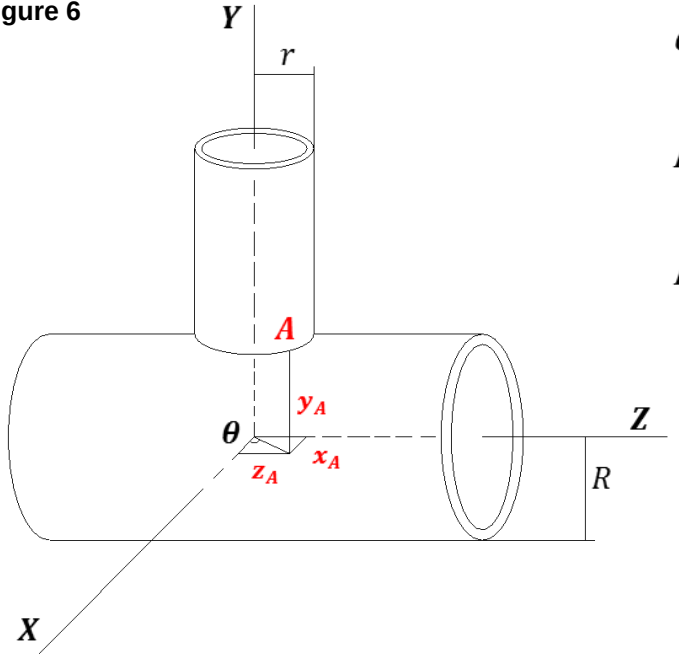

Chord equation:

$$x^2 + y^2 = R^2$$

Brace equation:

$$x^2 + z^2 = r^2$$

Intersection equation:

$$z^2 - y^2 = r^2 - R^2$$

Figure 7

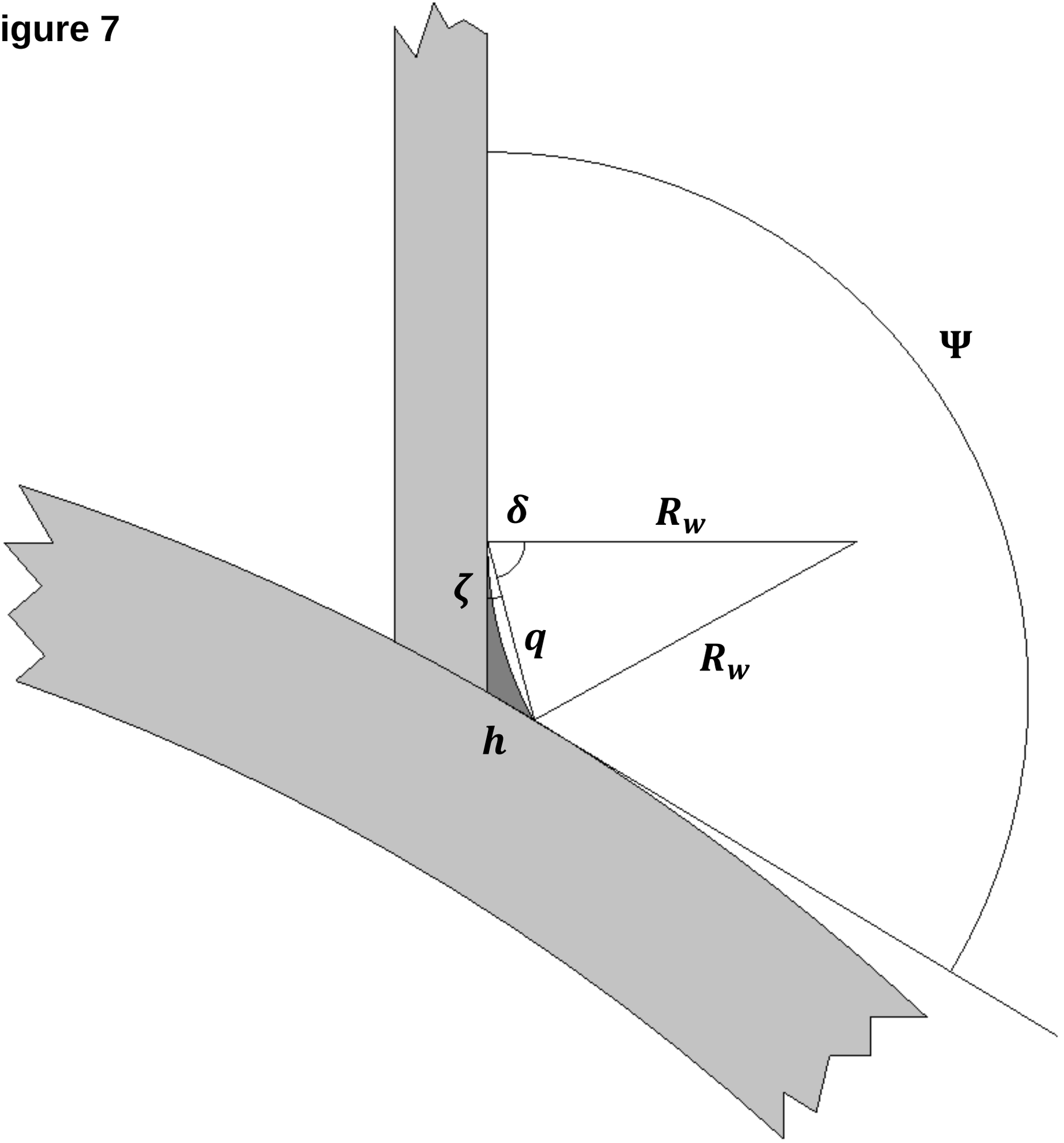

Figure 8

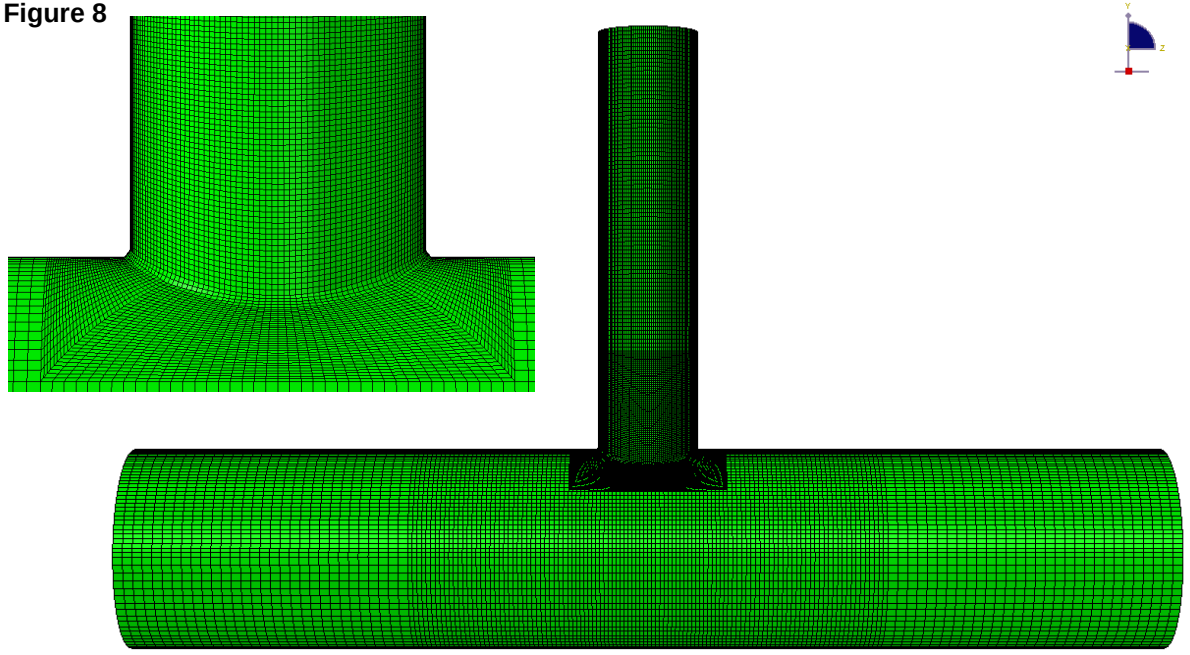

Figure 9

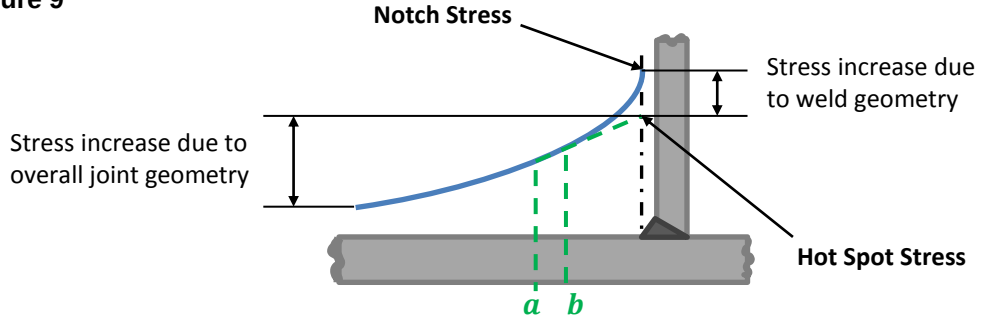
Notch Stress
Stress increase due to weld geometry
Stress increase due to overall joint geometry
Hot Spot Stress
a
b

Figure 10

$a = 0.2\sqrt{rt}$ (not smaller than 4mm)

$b_1 = 0.65\sqrt{rt}$

$b_2 = 0.4\sqrt[4]{rtRT}$

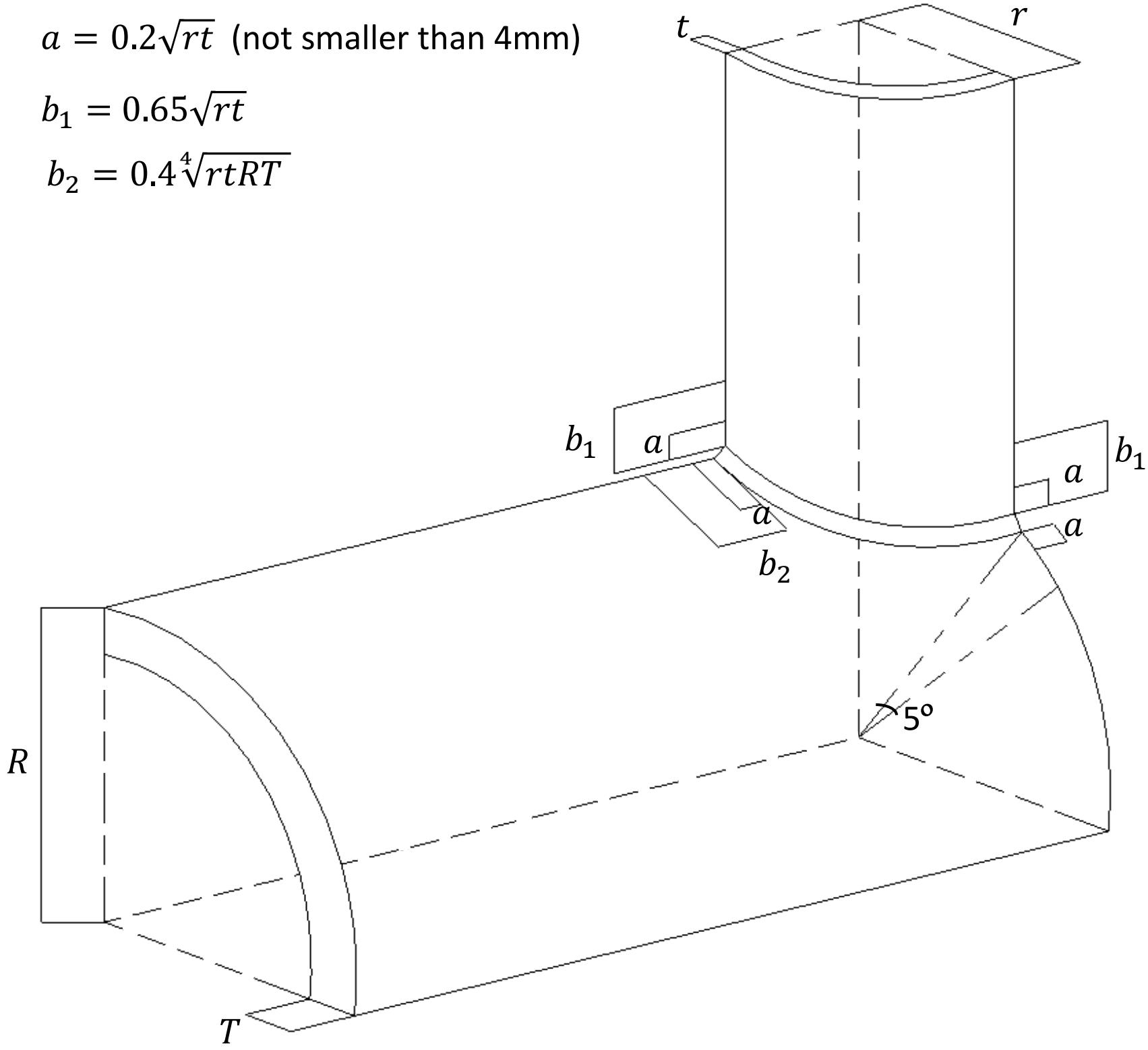

Figure 11

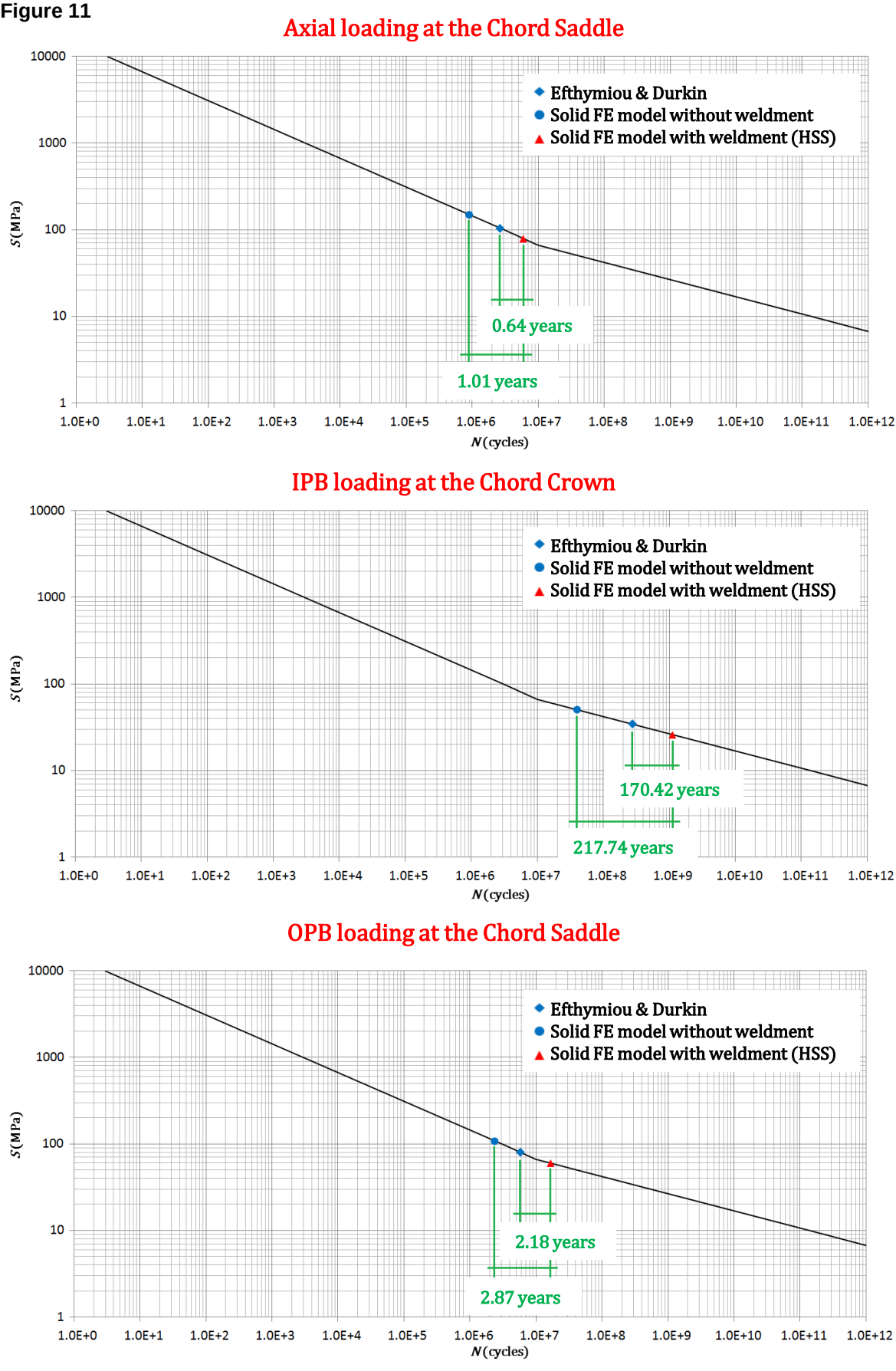
Axial loading at the Chord Saddle
Efthymiou & Durkin
Solid FE model without weldment
Solid FE model with weldment (HSS)
0.64 years
1.01 years
S (MPa)
N (cycles)
IPB loading at the Chord Crown
Efthymiou & Durkin
Solid FE model without weldment
Solid FE model with weldment (HSS)
170.42 years
217.74 years
S (MPa)
N (cycles)
OPB loading at the Chord Saddle
Efthymiou & Durkin
Solid FE model without weldment
Solid FE model with weldment (HSS)
2.18 years
2.87 years
S (MPa)
N (cycles)